



OPEN ACCESS

EDITED BY

Hans-Balder Havenith,
University of Liège, Belgium

REVIEWED BY

Honghua Lu,
East China Normal University, China
Duo Wu,
Lanzhou University, China

*CORRESPONDENCE

Hao Wang,
✉ hgoodspeed2008@163.com

SPECIALTY SECTION

This article was submitted to
Geohazards and Georisks,
a section of the journal
Frontiers in Earth Science

RECEIVED 12 September 2022

ACCEPTED 22 November 2022

PUBLISHED 19 January 2023

CITATION

Wang H, Yang A, Jiang S and Liu N
(2023), Reconstruction of a Holocene
landslide-dammed lake in the Yalong
basin, eastern Tibetan Plateau.
Front. Earth Sci. 10:1042581.
doi: 10.3389/feart.2022.1042581

COPYRIGHT

© 2023 Wang, Yang, Jiang and Liu. This
is an open-access article distributed
under the terms of the [Creative
Commons Attribution License \(CC BY\)](#).
The use, distribution or reproduction in
other forums is permitted, provided the
original author(s) and the copyright
owner(s) are credited and that the
original publication in this journal is
cited, in accordance with accepted
academic practice. No use, distribution
or reproduction is permitted which does
not comply with these terms.

Reconstruction of a Holocene landslide-dammed lake in the Yalong basin, eastern Tibetan Plateau

Hao Wang^{1*}, Anna Yang^{1,2}, Shengfan Jiang³ and Nannan Liu⁴

¹Institute of Mountain Hazards and Environment, Chinese Academy of Sciences, Chengdu, China, ²University of Chinese Academy of Sciences, Beijing, China, ³Emergency Management Agency of Laoshan District, Qingdao, China, ⁴Hennan Laboratory of Research for Central Plains Ancient Ceramics, Pingdingshan University, Pingdingshan, China

The failures of natural dams formed by landslides and glaciers in mountain areas have triggered the most destructive flood events on Earth. Outburst floods are effective agents in modifying landscapes, such as carving bedrock gorges and transporting surface masses. Reconstructing the ages and magnitudes of prehistoric landslide damming events allows us to capture the full range of frequencies and magnitudes of similar events and deepen our understanding of the interaction between large landslides and trunk rivers in tectonically active high-relief mountains. Previous studies have revealed many paleo-landslide-dammed lakes in the Yarlung Tsangpo River and its tributaries, the Jinsha River and the Min River. However, most studies associated with paleo-event reconstruction lack an estimation of the extent and volume of paleo-landslide-dammed lakes. The paleo-level of a landslide-dammed lake can be recorded in the variation in the sedimentary sequence and the geometry of the breach channel of a landslide dam. This information has not been fully exploited. In this study, we identified sedimentary evidence formed by an ancient landslide-dammed lake in the Liqiu River, a left-bank tributary of the Yalong River. The 12 exposures that we investigated mainly consist of typical clay or silt varves deposited in deep water and the Bouma sequence deposited by subaqueous turbidity flows, as well as climbing ripples that formed in a near-shore environment. Based on sedimentary analysis, we inferred that the minimal lake volume of this ancient lake was approximately $2.4 \times 10^8 \text{ m}^3$, corresponding to a lake level at 3,187 m a.s.l. The maximal lake extent derived from relict dam morphology reveals a lake volume of $3.2 \times 10^8 \text{ m}^3$ at the level of 3,200 m a.s.l. An initial drainage that occurred as the lake water overtopped the landslide dam was suggested to explain the small discrepancy in the lake level. The relict lake has remained stable over a long period of time and has accommodated continuous clay varve deposits. Furthermore, the optically stimulated luminescence dating results illustrate that the dammed lake initiated before 7.9 ka BP and persisted until at least 3.9 ka BP. The long-term cumulative coupled effect of tectonic movement and the rapid river incision rate provided favorable conditions for the failure of the Yuting landslide.

KEYWORDS

landslide-dammed lake, sedimentary evidence, optically stimulated luminescence dating, Yalong river basin, Holocene

1 Introduction

The damming of major rivers and consequent catastrophic outburst floods occurring in mountain regions are some of the most destructive geological hazards (Wang et al., 2022). It has been discovered that the majority of the most catastrophic floods on Earth originate from the failure of landslides or glacier dams (Carling, 2013; Liu et al., 2019; Baker, 2020; Bazai et al., 2021; Yang et al., 2022), extending our knowledge of the scale and frequency of known mass-transport events. These floods rapidly modify planetary surfaces and carved large bedrock canyons (Baker, 2009; Baynes et al., 2015; Larsen and Lamb, 2016). Landslides or glaciers can construct natural dams with both long and short durations. It is possible that repeated blockage of major rivers by landslides or surging glaciers may profoundly hinder retrogressive river erosion and effectively interrupt the long-term evolution of fluvial geomorphology (Korup and Montgomery, 2008; Korup et al., 2010). Using the continually increasing data from this region to reconstruct ancient extreme landslide damming events that have not been observed in modern times, we can capture the full range of the frequency–magnitude curve. Statistically, we can quantitatively evaluate the impact of landslide damming on the long-term incision of large rivers in this region and explore how slope processes, such as landslides, correspond to river incision driven by tectonic uplift. Moreover, this evaluation can provide special insight into modern hazard prevention and management under varying climatic and tectonic conditions.

The eastern Tibetan Plateau features extremely high river incision rates, high relief, and seismic activity. The unique geological, geomorphological, and climatic conditions in this region facilitate the prevailing of large landslides and consequent cascade events, such as the Yigong events in 2000 (Delaney and Evans, 2015) and Baige events in 2018 (Liu et al., 2021; Yi et al., 2022). Previous studies have revealed that the watercourses of the Yarlung Tsangpo River and its tributaries (Liu et al., 2015; Wang H. et al., 2019; Hu et al., 2022; Wang et al., 2022; Yang et al., 2022) and the Jinsha River (Chen et al., 2008; Zhang et al., 2011; Chen et al., 2013; Wang et al., 2014; Liu et al., 2018; Bao et al., 2020; Li et al., 2020) have been frequently blocked by landslides in the late Quaternary. The most recent case of a landslide-dammed lake in the Yalong River occurred on 8 June 1967. The landslide blocked the river and formed a lake with a volume of $6.8 \times 10^8 \text{ m}^3$, which breached on 17 June and gave rise to an outburst flood of $5.3 \times 10^4 \text{ m}^3/\text{s}$ (Chen et al., 1992). However, most studies associated with paleo-event reconstruction lack an estimation of the extent and volume of paleo-landslide-dammed lakes, such as Ding et al. (2021). The

paleo-level of a landslide-dammed lake can be recorded in the variation in the sedimentary sequence and the geometry of the breach channel of a landslide dam. This information has not been fully exploited. We conducted a detailed investigation of the Yalong River and identified an ancient landslide-dammed lake of long duration in a tributary of the Yalong River—the Liqiu River. Based on this illustrative example, we highlight the sedimentary characteristics of the remnant sediment of a paleo-landslide-dammed lake and propose an approach to reconstruct the lake volume based on sedimentary analysis and geomorphic imprints. Finally, by combining optically stimulated luminescence (OSL) dating, it is possible for us to re-establish the evolutionary history of this river-blocking event.

2 Regional setting

The watercourse of the Yalong River follows a series of north–south-oriented faults in the Hengduan Mountain(s). The upper and middle reaches of the Yalong River are tectonically situated in the Ganzi–Aba fold belt and are bounded by the Xianshuihe fault and the Batang fault. Triassic low-grade metamorphic rocks dominate the lithology of the study area and mainly consist of sandstone rocks intercalated with granite intrusions, Permian carbonate, shale, and ophiolitic melanges. The lower reach of the Yalong River is composed of Paleozoic carbonates and low-grade metamorphic rocks, with minor basalt, gneiss, schist, granite, and conglomerate.

The Yalong River ($26^{\circ}32'–33^{\circ}58'N$, $96^{\circ}52'–102^{\circ}48'E$) originates from the Bayan Har Mountains at an elevation of nearly 5,000 m and is the largest tributary of the Jinsha River in the eastern Tibetan Plateau, with a total basin area of approximately 136,000 km² and a mainstream length of 1,571 km (Li et al., 2014; Wang Y. et al., 2019). The Yuting landslide-dammed lake is located in the Liqiu River basin, which is one of the major tributaries of the Yalong River (Figure 1). The Yalong River, with an average annual discharge of 1914 m³/s, is mainly supplied by precipitation occurring during the wet season (June to October), which accounts for 75% of the precipitation (Feng et al., 2008). Due to the influence of the monsoon climate, the average annual precipitation entering the Yalong River is 500–2,470 mm, and the average annual temperature range in the basin is $-4.9^{\circ}\text{C}–19.7^{\circ}\text{C}$ (Li et al., 2014; Wang Y. et al., 2019). The Liqiu basin has a total area of 5,828 km², with a length of 203.5 km. The relief from the river head to the confluence with the Yalong River is approximately 2078 m, giving an average channel gradient of 10.21%. The discharge of the Liqiu River is absent.

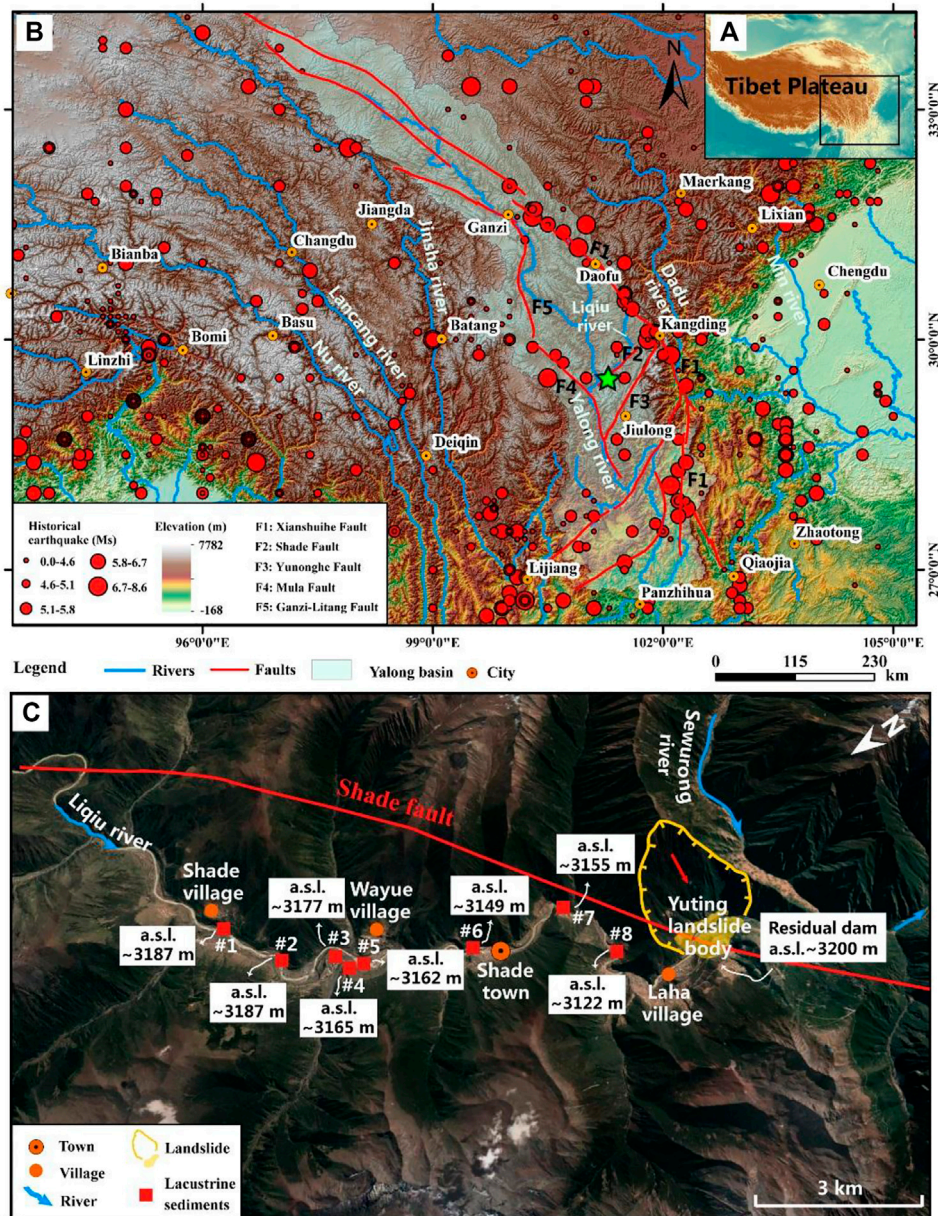


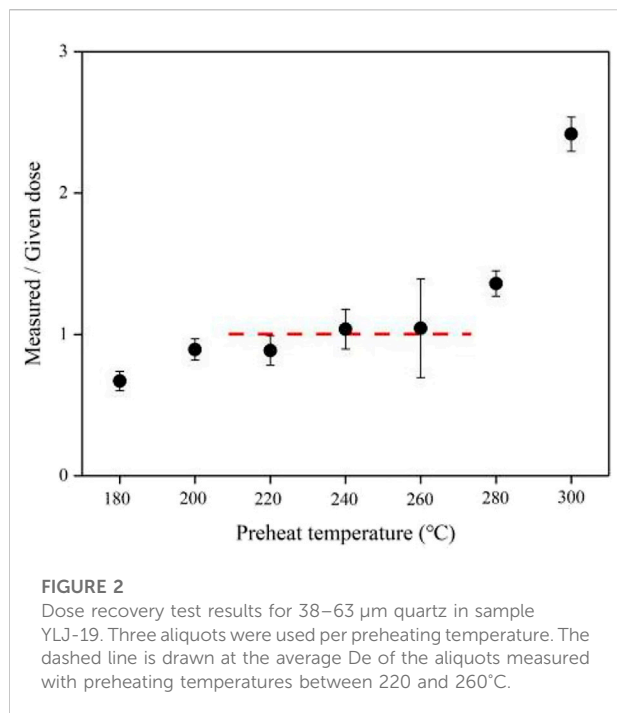
FIGURE 1 Study area and Yuting landslide-dammed lake. (A) Map of the Tibetan Plateau. (B) Location of the study area in the eastern Tibetan Plateau. Filled red circles represent historical earthquakes. The green pentagram in (A) represents the location of the Yuting landslide-dammed lake. (C) Satellite image of the Yuting landslide-dammed lake. Satellite image is from Google Earth.

3 Materials and methods

3.1 Facies analysis

To define sedimentary facies, detailed analyses of sedimentary characteristics in lacustrine exposures were carried out at eight exposures in the Liqiu catchment

(Figure 1B). In the sedimentary sequences, we logged some changes in grain size, bed thickness, bed geometry, bed contacts, and internal sedimentary structures (Russell and Arnott, 2003; Wang H. et al., 2019) and used photographs and lines to record details and show differences in sedimentary facies at each outcrop, which were helpful for differentiating lacustrine deposits from other deposits.



3.2 Luminescence dating

Twelve samples were collected from section #1 (LQ-1), section #5 (LQ-5), and section #6 (LQ-6) for OSL dating to estimate the chronological limits of the studied landslide-dammed lake (Figures 2, 3). Sample preparation (chemical extraction of pure quartz grains from sediment and OSL measurements) was performed under subdued red light based on the specific collection, pretreatment steps, and measurement procedure reported in Lai and Ou (2013). All the processes were completed in the OSL laboratory of the Institute of Mountain Hazards and Environment, which is equipped with a Lexsyg research reader.

Because of the possibility of exposure in the collection, approximately 3 cm of material at each end of the sample tubes was removed and reserved for environmental dose rate and water content measurements. The environmental dose rate was calculated from measurements of radioactive element concentrations of the surrounding sediment with a small contribution from cosmic rays. U and Th concentrations and K contents for all samples were measured using neutron activation analysis in the Xi'an Center of the Geological Survey, China. The cosmic ray dose rate was calculated from the burial depth of the samples and the altitude and latitude of the study area (Prescott and Hutton, 1994). The α efficiency value of 0.035 ± 0.003 was adopted during the dose rate calculation (Lai and Brückner, 2008). The observed water contents of samples from lacustrine sediments ranged from 5% to 17%, with an average water content of 13%. Given that the section has been exposed to sand excavation for a long time, the uncertainty of water content changes after burial, and the slight loss of sample moisture that occurs

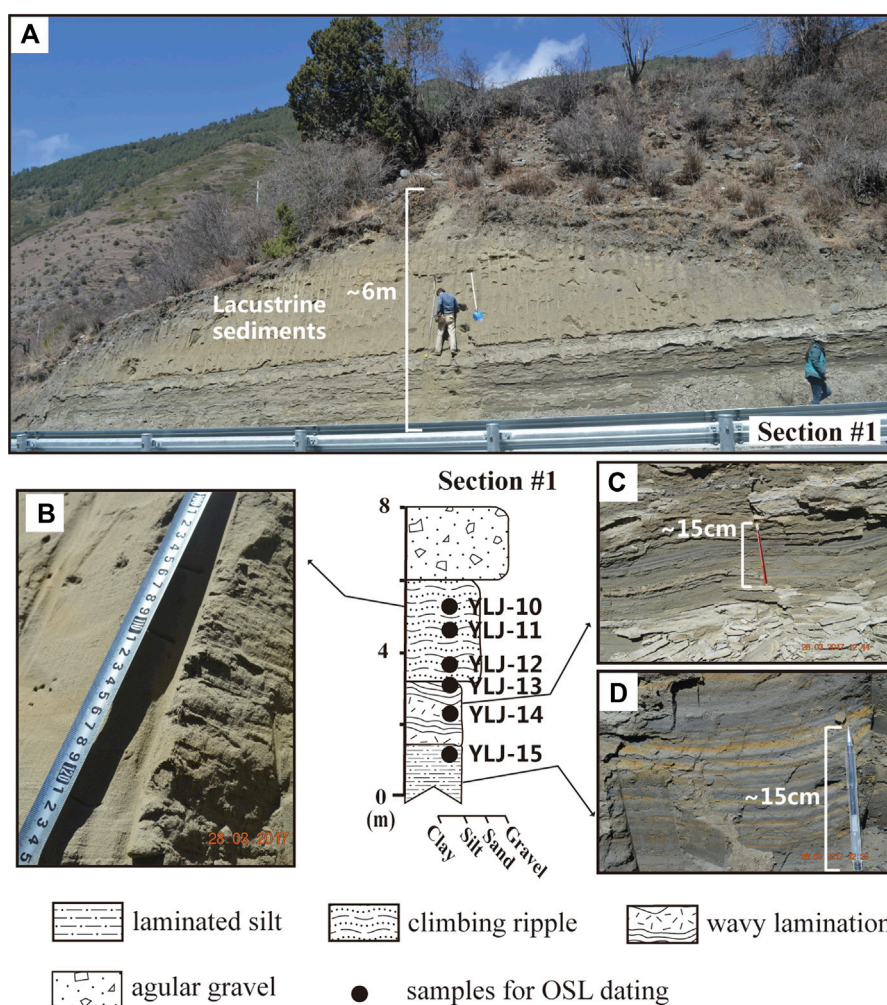
naturally during sampling and transport, a lifetime average water content of $15 \pm 5\%$ was used for dose rate calculations for lacustrine samples (Liu et al., 2015; Wang H. et al., 2019).

OSL measurements were performed on Lexsyg research readers equipped with blue LEDs ($458 \pm 5 \text{ nm}$, $\sim 100 \text{ mW/cm}^2$) and infrared LEDs ($850 \pm 20 \text{ nm}$, $\sim 300 \text{ mW/cm}^2$). A combination of the single-aliquot regenerative-dose (SAR) protocol (Murray and Wintle, 2000) and the standard growth curve (SGC) method (Roberts and Duller, 2004; Lai, 2006) was applied to determine the equivalent dose (D_e) of 38–63 μm quartz grains. Twenty aliquots were measured for each sample, of which six to eight aliquots were used for D_e determinations using SAR to construct the SGC. Twelve to fourteen additional aliquots were measured for their natural (LN) and test dose (TN) OSL signals under the same measurement conditions as those of SAR. The D_e value was obtained by matching the test dose-corrected natural OSL signal in the SGC. Samples for which the difference between SGC D_e and SAR D_e was within 10% (Table 2) suggest that the D_e results determined by the SGC are in agreement with those determined by the SAR protocol (Lai et al., 2014) and that the SGC could be used for D_e determination. The final D_e value was the mean of the SAR D_e s and the SGC D_e s. Otherwise, the mean value of SAR D_e was used for dating (Liu et al., 2012). Using the combined approach, it is possible to construct standardized growth curves by parts of standard SAR measurements; then, the remaining accurate estimates of D_e can be obtained based solely on measurements of Ln and Tn, which can effectively speed up the measurement process and reduce the measurement time (Roberts and Duller, 2004; Lai, 2006).

To check the suitability of the SAR protocol for D_e determination, a dose recovery test (Murray and Wintle, 2000) was conducted for sample YLJ-19 (Figure 2). Before the dose recovery test, the OSL single from each aliquot was bleached with a solar simulator using a certain exposure time, and the residual natural doses were measured to ensure that they had reached a negligible level. Subsequently, they were given a known dose close to the equivalent dose, with preheating temperatures increasing from 180 to 300 °C at an interval of 20 °C. For each preheating temperature point, three aliquots were used for D_e determination (Murray and Wintle, 2000; Lai et al., 2009; Li et al., 2020). For sample YLJ-19, a plateau was observed for temperatures from 220 to 260 °C, and the average measured-to-given dose ratio was close to 1 ($n = 3$). Therefore, the optical measurements were performed after heating at a temperature of 260 °C for 10 s for natural and regenerative doses and after preheating at a temperature of 220 °C for 10 s for test doses.

4 Results

Careful investigation in the field revealed eight lacustrine exposures along the No. S215 Highway associated with landslide-

**FIGURE 3**

Detailed sedimentary logs and photographs of lacustrine sediment in section #1 at the Yuting landslide-dammed lake. Solid black circles and YLJ symbols represent the depth and number of OSL dating samples. (A) Panorama picture of section #1. Note that the maximum exposed thickness is 6 m. (B) Close-up photograph of climbing ripples on the top of section #1. (C) Close-up of wavy lamination in section #1. (D) Typical annual lacustrine varve couplet.

dammed lakes in the lower reach of the Liqiu River near Shade town. We analyzed the evolution of this landslide-dammed lake based on sedimentary interpretation and OSL dating. The elevation of the sedimentary association in the reservoir area and the morphology of the body of the landslide dam were further used to reconstruct the dam height and volume of lake water.

4.1 Characteristics of lacustrine deposition

The relative locations of the eight exposures of lacustrine sediments lie between the Shade and Laha villages (Figure 1C). Their coordinates and elevations are listed in Table 1. All of the

exposures are commonly characterized by coupled varve laminae, comprising couplets of a light-colored summer-deposited coarse-grained silt layer and a dark winter-deposited fine-grained clay layer with mm- to cm-thick beds (Figures 3–6). Continuous varve sediments contain multiple seasonal laminae with obvious contrasts in color, grain size, and bed thickness (Zolitschka et al., 2015). Locally, the clay varves in most exposures, including section #1, section #3, section #5, and section #8, are slightly wavy (Figures 3C, 4A,4B). Another distinguishing characteristic is the laminated carbonate (Figure 4C), which alternates between light-colored silt and dark carbonate-rich clay, with a maximum lateral extension of a few tens of meters, ranging from a few centimeters to some decimeters thick. The dark winter-deposited carbonate clay in

TABLE 1 The elevations of lacustrine exposures and simple descriptions of sedimentary characteristics.

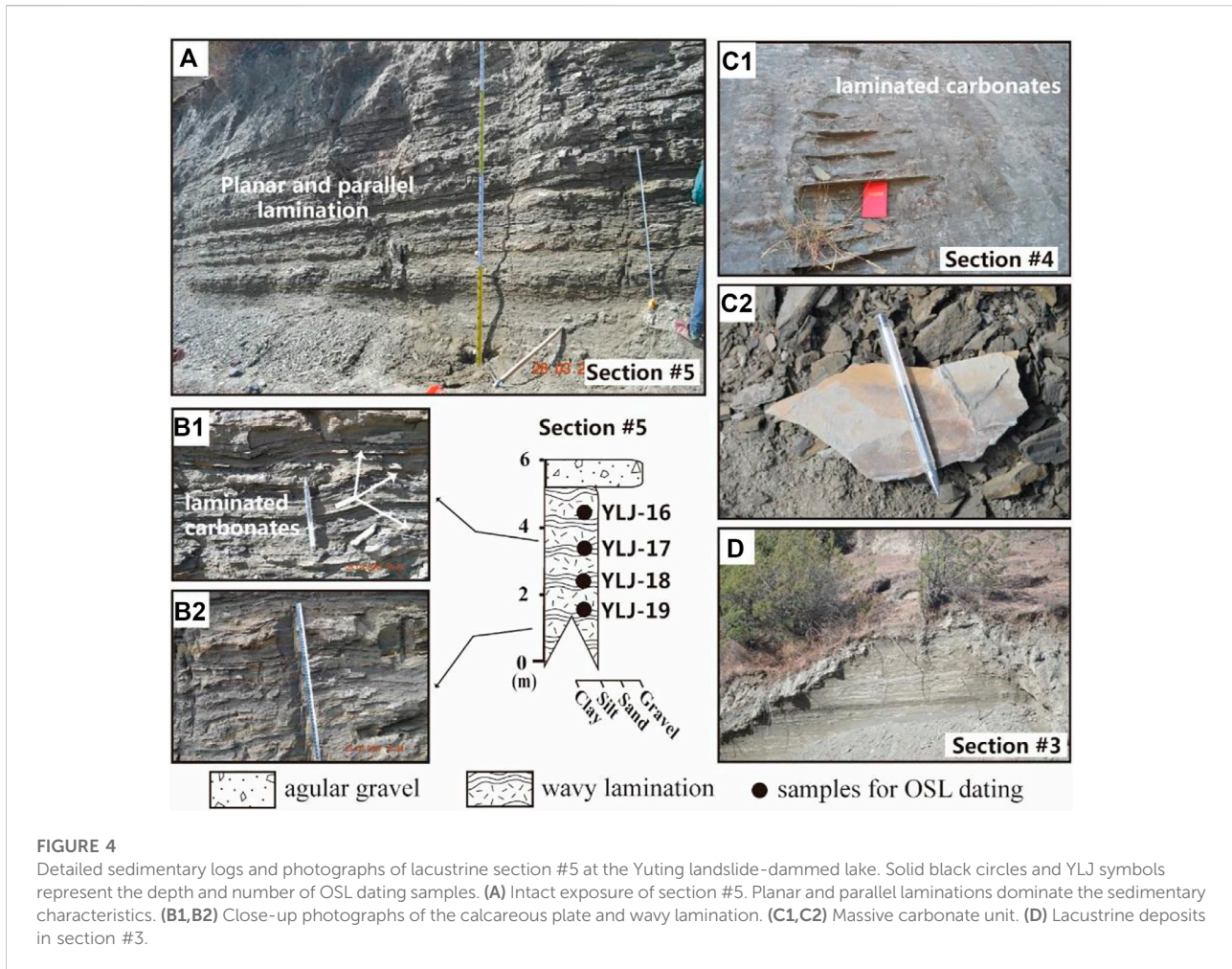
Exposure ID	Coordinate	Top elevation (a.s.l.)	Relative height above river (m)	Sedimentary description
Section #1	29°40'10.87"N, 101°24'21.98"E	3,187	14	In addition to Shade village, the exposure height is approximately 6 m (Figure 3C). The upper part is 2 m thick and contains climbing ripples of fine sand and silt. The lower part, which is 3 m thick, consists of wavy lamination and typical lacustrine clay varves. Six OSL samples, YLJ-10–YLJ-15, were collected from this section.
Section #2	29°39'47.62"N, 101°23'32.34"E	3,187	25	Approximately 1.5 km downstream from section #1. The whole exposure consists of silty clay varves.
Section #3	29°39'5.84"N, 101°23'12.26"E	3,177	27	In addition to the S215 Highway, the exposure is 18 m thick. The lower 16-m-thick part is composed of clay varves (Figure 4D).
Section #4	29°38'59.10"N, 101°23'4.19"E	3,165	19	Approximately 1.5 km downstream from section #3. The lacustrine sediment is approximately 9.8-m thick and mainly consists of carbonate-rich, well-cemented, and dark-colored clay varves (Figure 4C).
Section #5	29°38'53.27"N, 101°22'54.74"E	3,162	16	The opposite bank of Wayue village. This exposure is approximately 5.5 m high and consists of silty clay varves. The lamination is slightly wavy. Four OSL samples, YLJ-16–YLJ-19, were collected from this section (Figures 4A,B).
Section #6	29°37'32.52"N, 101°22'19.26"E	3,149	14	Close to Shade town. The exposure is approximately 12.1 m. The middle 2-m-thick part is a typical Bouma sequence consisting of laminated sand and silt and climbing ripples. Two OSL samples, YLJ-20 and YLJ-20, were collected from this section (Figure 4A,B).
Section #7	29°36'17.55"N, 101°22'4.55"E	3,155	38	Approximately 2.3 km downstream from section #6. The exposure contains 2.3-m-thick clay varve drapes on the toe slope. Intraclasts can be observed (Figure 6).
Section #8	29°36'0.51"N, 101°21'6.62"E	3,122	16	In addition to the S215 Highway, the lacustrine sediment of clay varves is 8.6 m thick. The angular colluvial sediment that is 4.6 m thick overlies the lacustrine varves. The lower 16-m-thick part is composed of clay varves (Figure 5A).

these carbonate laminations is well cemented. We identified only a 5–20-cm-thick layer of climbing ripples occurring in the upper parts of section #1, which are made up of light-colored silt to sand. In successive laminae, nearly all climbing ripples were not a perfect superposition but rather a minor displacement of the ripple crests (Figure 3B).

Another major variant in the sedimentary association of the Yuting landslide-dammed lake is the Bouma sequences (Ta–Te) in section #6 (Cantero et al., 2012; Wang H. et al., 2019). As Figure 4B shows, the uppermost part (Ta) of section #6 is composed of debris flow deposits, which are mainly massive mixtures of angular and subangular gravel and sand that lack sedimentary structures. Intervals Tb to Tc tend to be sand, showing layers of climbing ripples that are interbedded with laminated sand beds. The Bouma sequence is introduced in detail in Cantero et al. (2012). Ferromanganese nodules with circular shapes can be locally observed inside the laminated varves in the upper parts of section #7 (Figure 6C). Small faults in laminated clay can be occasionally observed (Figures 6B,C).

The components of lacustrine deposition are controlled by the catchment geology and climate conditions (Zolitschka

et al., 2015). The geological conditions are usually in a stable state and do not alter the sedimentation process during the lifetime of a lake. In contrast, climatic conditions vary over longer timescales and can produce a series of seasonally contrasting and characteristic laminae (Zolitschka et al., 2015; Lettéron et al., 2018). The necessary precondition for forming an annual lacustrine varve couplet is a seasonally varying sediment flux into the lake (Zolitschka et al., 2015). The color of varve laminae commonly adjusts following variations in the organic matter content. A lighter color, for instance, indicates a low content of organic matter. Simultaneously, a regularly bedded succession is indicative of perennial subaqueous environments (Lettéron et al., 2018). The discrepancy in the grain size of a varve couplet is due to the variation in the seasonal runoff that carries suspended sediment into the lake. Coarser particles (sand and coarse silt) are deposited immediately as they enter the lake, whereas finer materials (silt and clay) remain in suspension for a longer time. Accordingly, a varve couplet is typically composed of both a coarse-grained layer and a fine-grained lamina (Zolitschka et al., 2015; Wang H. et al., 2019).



The wavy lamination of clay may form as a result of settling from suspension onto an undulating lake bottom substrate or uneven sedimentation of the suspended matter. The laminated carbonate may indicate enhanced carbonate dissolution and carbonate input into the lake from the surroundings. The accumulation of lacustrine carbonates is ascribed to a massive influx of carbonate, including bedload, suspended load, and dissolved load. The widespread carbonate deposits reveal a stable lacustrine environment and internal lake processes, which determine whether precipitation or deposition of carbonates can be well preserved (Lettéron et al., 2018). The deposition of climbing ripples in section #1 implies the existence of long-lasting unidirectional flows (Lang and Winsemann, 2013). In view of the fact that the existence of climbing ripples requires deposits to be transported as bedload, the multiple occurrences of climbing ripples indicate a relatively shallow lake environment (Wang H. et al., 2019).

The Bouma sequence in Figure 5B2 is a typical product of high-density turbidity flows, such as subaqueous debris flows.

The Ta-Te units that form from bottom to top indicate the waning process of the flow (Cantero et al., 2012). The rapid settlement of coarse-grained gravel in the turbidity flow gave rise to the Ta unit. Parallel sand laminations in the Tb unit indicate bedload reworking as sediment settles, and the climbing ripple layers of the Tc unit imply high sedimentation rates under a lower flow regime during phases of reduced discharge (Lang and Winsemann, 2013; Lang et al., 2017; Winsemann et al., 2018). Laminated silts (Td) may occur due to silt suspension fallout of turbulent flow (Wang H. et al., 2019). The Te unit resulted from the settling of the finest clay component in the final stage of the turbidity flow process. The growth of ferromanganese nodules in Figure 6C requires a sustained source of Fe and Mn from the underlying sediment porewater. Ultimately, the Fe and Mn derived from the sediments are released to the sediment porewater by reductive dissolution of their respective oxides and hydroxides, which is a common diagenetic process in lake sediments. Once in the porewater, the dissolved Fe (II) and Mn (II) can migrate by advection and/or diffusion upwards to

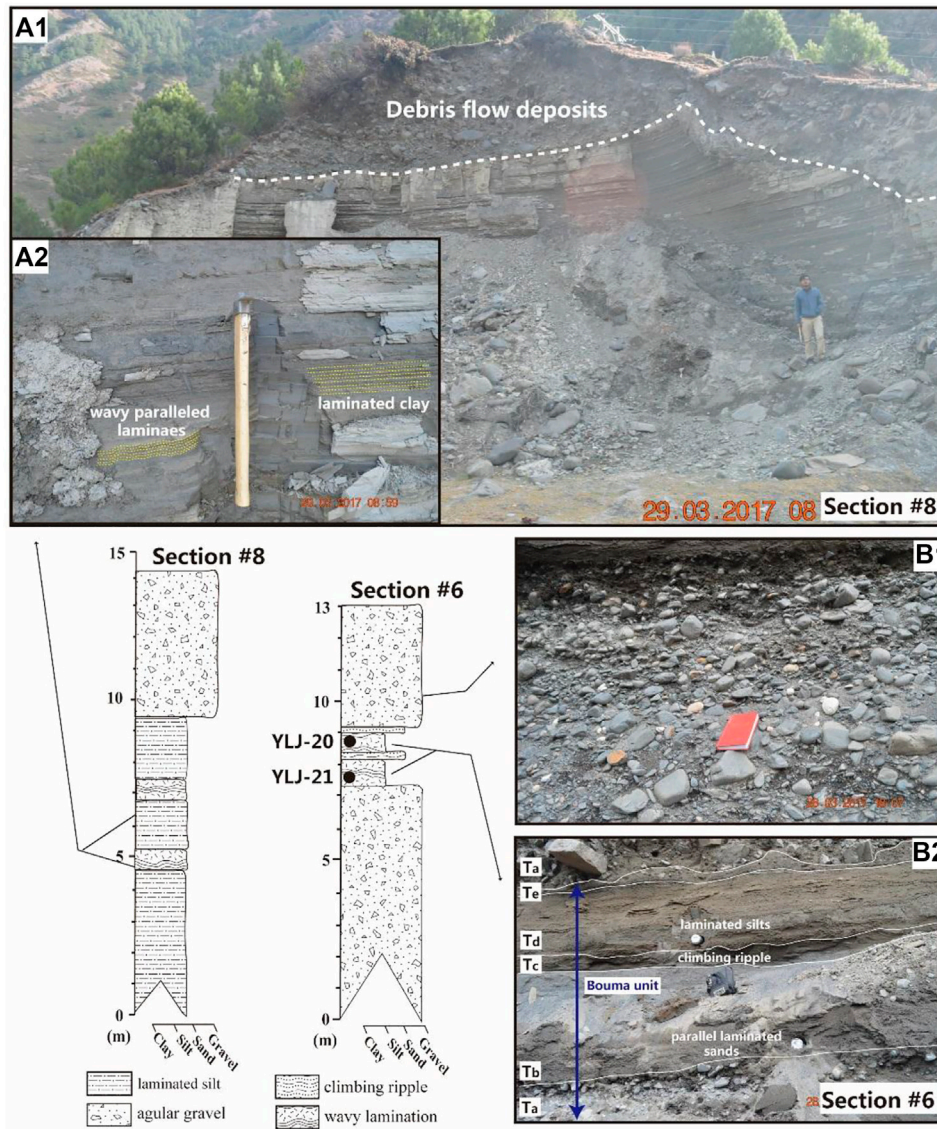


FIGURE 5
 Detailed sedimentary logs and photographs of lacustrine sections #6 and #8 in the Yuting landslide-dammed lake. (A1) Macroscopic sedimentary features of section #8. (A2) Wavy parallel laminae and climbing ripples from section #8. (B1) Debris flow sediments in the upper part of section #6. (B2) Typical Bouma sequence in the middle of section #6.

the sediment–water interface and oxidize rapidly by chemical or biologically mediated mechanisms (Hayles et al., 2021). The small faults of laminated clay in Figures 6B,C may result from the slight slump of the lacustrine slope responding to the postevent incision by the river.

Overall, except for section #6, the typical vertically continuous clay or silt varve deposition that developed in all lacustrine exposures represents a stable depositional environment in relatively deep water. The climbing ripples in section #1 emerge in near-shore shallow water. We did not observe any alternation of varve and climbing ripple units in

the sedimentary sequence of all exposures, which implies that the lake remained stable for a long period of time.

4.2 Landslide volume estimate

The landslide dam of the Yuting landslide-dammed lake was generated from a bedrock ridge to the east of the Liquiu River, forming an obvious negative relief (Figure 1C). The sliding mass exhibits expansion toward the west, hitting the opposite side of the mountain and forming a landslide dam. Based on the

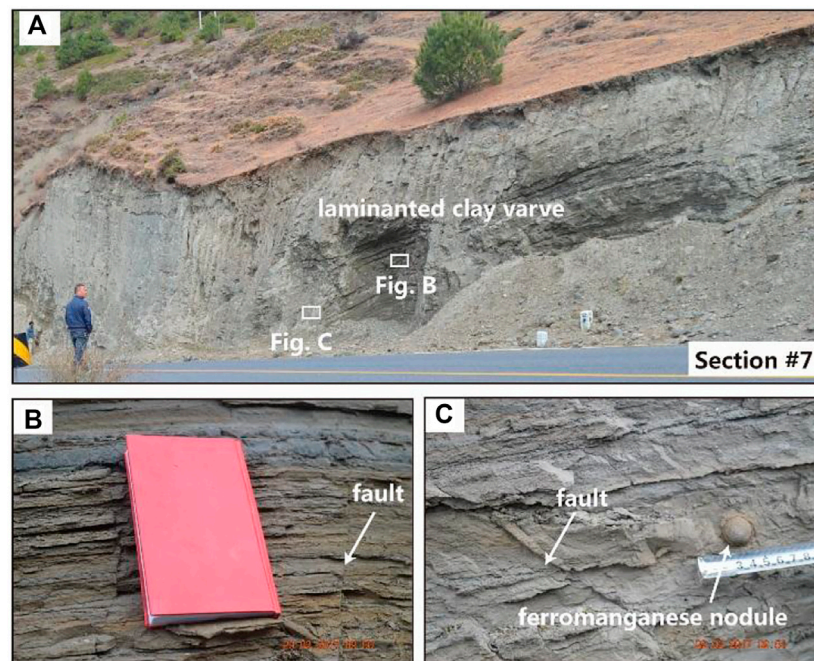


FIGURE 6

Macroscopic and detailed sedimentary characteristics of section #7, mainly including soft-sediment deformation structures. (A) Panorama picture of section #7. (B) Close-up photograph of clay lamination in section #7. (C) Close-up photograph of ferromanganese nodules in section #7.

geometry of the landslide deposit, we calculated an area of approximately $1.36 \times 10^6 \text{ m}^2$. The estimated volume V of a given landslide of area A depends on a scaling exponent γ and intercept α (Simonett, 1967):

$$V = \alpha A^\gamma$$

Taking a γ value of 1.41 and a loga value of 0.23, as proposed for bedrock landslides in the Himalaya by Larsen et al. (2010), the volume of the Yuting landslide is calculated as $1.02 \times 10^8 \text{ m}^3$.

4.3 OSL dating results

The OSL dates for lacustrine sediments are summarized in Table 2. Twelve samples for OSL dating were collected from section #1, section #5, and section #6. The OSL signal of the natural (N), regeneration (0 Gy), and test (TD) doses for sample YLJ-17 are shown in Figure 7A. Both the natural quartz OSL and regeneration dose signals attenuate rapidly to the background level within the first second of stimulation, indicating that the quartz OSL signal is dominated by the fast component (Steffen et al., 2009; Fan et al., 2011). The growth curve of eight individual aliquots of the same samples can be well fitted using an exponential plus linear function (Figure 7B). The recuperation of the natural signal for all 108 quartz aliquots from 12 quartz samples is less than 5% (Figure 7C). For

recycling ratios, most of the samples are between 0.9 and 1.1 (Figure 7C), and we rejected aliquots that did not meet the criteria. According to these standards, there are not enough aliquots to calculate D_e for samples YLJ-12 and YLJ-14.

The extent of grain bleaching prior to burial is a basic concern in luminescence dating (Mangerud et al., 2001; Wallinga, 2002). All samples reported here were collected from lacustrine sediments, which means that the problem of partial bleaching may exist, as underwater zeroing is slower (Mangerud et al., 2001; Wallinga, 2002). According to the Abanico plot (Figure 8), the tight and symmetric distribution of most ages favors basically zeroing the OSL signal (Murray et al., 1995; Olley et al., 1998; Olley et al., 1999). If samples have been poorly bleached prior to burial, the OSL dates may tend toward a range skewed to older ages, which may yield a higher uncertainty than expected, as we could not assess the extent of bleaching of grains for each individual sample. Moreover, the overdispersion (OD) of D_e can be used to illustrate incomplete zeroing during deposition, and samples with values greater than 20% are not considered (Yang et al., 2022). YLJ-19 shows the highest overdispersion (32.61%), which may be due to the problem inherent in OSL dating of young sediments (Lapointe et al., 2019). Young sediments are universally characterized by low luminescence sensitivity (Figure 7D) due to the short sedimentary history of young orogenic belts (Preusser et al.,

TABLE 2 Paleodose, dose rate, and ages obtained from quartz extracted from deposits.

Section	Sample ID	Depth (m)	K (%)	Th (ppm)	U (ppm)	Water content (%)	Dose rate (Gy/ka)	Aliquot numbers	SAR De (Gy)	SGC De (Gy)	Final De (Gy)	Age (ka)	OD (%)
1 [#]	YLJ-10	2.9	2.09 ± 0.06	20.1 ± 0.5	2.89 ± 0.1	15±5	4.31 ± 0.30	8 ^a ± 12 ^b	15.61 ± 1.47	16.93 ± 1.11	16.40 ± 0.88	4.1 ± 0.4	24.50
	YLJ-11	3.7	2.21 ± 0.06	16.6 ± 0.5	3.28 ± 0.1	15±5	4.23 ± 0.29	6 ^a ± 14 ^b	15.04 ± 1.77	15.88 ± 0.98	15.63 ± 0.85	3.9 ± 0.3	23.60
	YLJ-12	4.6	2.19 ± 0.07	19.2 ± 0.5	2.62 ± 0.1	15±5	4.21 ± 0.29	—	—	—	—	—	—
	YLJ-13	5.1	2.25 ± 0.07	16.1 ± 0.4	3.37 ± 0.1	15±5	4.22 ± 0.30	7 ^a	21.32 ± 1.19	24.16 ± 1.55	21.32 ± 1.19	5.4 ± 0.5	13.44
	YLJ-14	5.9	2.38 ± 0.07	19.7 ± 0.5	4.12 ± 0.1	15±5	4.48 ± 0.31	—	—	—	—	—	—
	YLJ-15	6.9	2.34 ± 0.07	17.7 ± 0.5	3.28 ± 0.1	15±5	4.09 ± 0.29	7 ^a	24.82 ± 1.69	34.60 ± 1.70	24.82 ± 1.69	6.1 ± 0.6	16.63
5 [#]	YLJ-16	1.4	2.37 ± 0.07	16.5 ± 0.4	3.23 ± 0.1	15±5	4.16 ± 0.28	8 ^a ± 12 ^b	21.24 ± 1.58	22.58 ± 1.38	22.04 ± 1.03	5.3 ± 0.4	19.63
	YLJ-17	2.4	2.42 ± 0.07	15.2 ± 0.4	3.20 ± 0.1	15±5	4.07 ± 0.28	8 ^a ± 12 ^b	32.28 ± 3.60	31.94 ± 2.77	32.08 ± 2.14	7.9 ± 0.8	28.97
	YLJ-18	3.2	2.8 ± 0.08	19.2 ± 0.5	3.01 ± 0.1	15±5	4.59 ± 0.31	8 ^a ± 12 ^b	35.36 ± 2.01	34.96 ± 1.44	35.12 ± 1.15	7.7 ± 0.6	13.38
	YLJ-19	4.2	3.15 ± 0.09	24.7 ± 0.6	2.93 ± 0.1	15±5	5.21 ± 0.37	8 ^a ± 12 ^b	33.66 ± 5.82	33.45 ± 2.49	33.54 ± 2.67	6.4 ± 0.7	32.61
6 [#]	YLJ-20	4.2	3.37 ± 0.06	14.45 ± 0.7	4.40 ± 0.1	15±5	5.76 ± 0.40	6 ^a	29.79 ± 0.85	16.37 ± 1.29	29.79 ± 0.85	5.2 ± 0.4	6.68
	YLJ-21	5.2	2.10 ± 0.08	15.2 ± 0.7	2.71 ± 0.1	15±5	3.63 ± 0.26	8 ^a ± 12 ^b	16.43 ± 1.18	17.80 ± 1.60	17.25 ± 1.05	4.8 ± 0.4	24.26

^aAliquot numbers using the SAR protocol.

^bAliquot numbers using the SGC protocol. OD is the overdispersion (%) of De values for each sample.

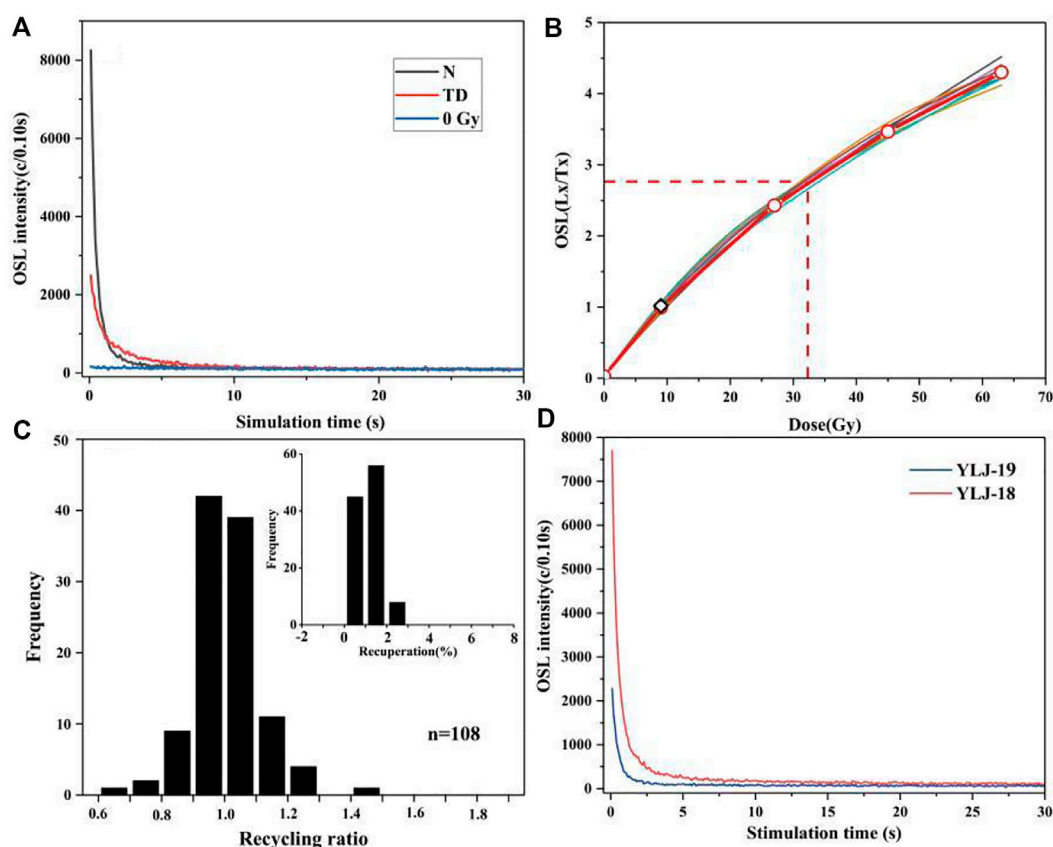


FIGURE 7

Luminescence characteristics of sample aliquots. (A) Decay curves of the OSL signals for sample YLJ-17; (B) growth curves of the OSL signals obtained using the SAR protocol for sample YLJ-17. The data were fitted using an exponential plus linear function. The thick red curves represent the fitted standard growth curve; diamonds and circles represent regeneration OSL signals, where circles represent R1~R5 and diamonds represent R1'. The square and dotted red lines indicate the sensitivity-corrected natural signal; (C) recycling ratios and recuperation values of all quartz aliquots; (D) decay curves of OSL signals for samples YLJ-18 and YLJ-19.

2005; Preusser et al., 2006; Pietsch et al., 2008; Preusser et al., 2009) and yield less imprecise ages. The possibility of partial bleaching cannot be excluded even if the OD is relatively low (e.g., <20%), and the ages should be used as maximum ages.

In total, we obtain ten OSL ages of lacustrine sediment deposited in the Yuting landslide-dammed lake (Table 1; Figure 8A). The oldest age of 7.9 ± 0.8 ka BP (YJL-17) is present in section #5. Because we failed to identify and date the lowest contact of lacustrine sediment, YJL-17 simply indicates the Yuting landslide-dammed lake formed before 7.9 ± 0.6 ka BP. The youngest lake deposition occurred in section #1, including YLJ-10 of 4.1 ± 0.4 ka BP and YLJ-11 of 3.9 ± 0.3 ka BP, implying that the water depth of the Yuting landslide-dammed lake at section #1 was shallow and close to its end around 3.8–3.9 ka BP (Table 2). Consequently, it can be deduced that persistent deposition of consecutive lacustrine sediments was continuing within a lifespan of

at least 4.0 ka. The OSL dating results illustrate that the Yuting landslide-dammed lake initiated before 7.9 ka BP and at least persisted until 3.9 ka BP. This chronological limit should be considered as the minimal lifespan of the Yuting landslide-dammed lake, which may have formed earlier and persisted longer.

5 Discussion

5.1 Evolution of the Yuting landslide-dammed lake

On most occasions, the top elevations of lacustrine sediments are used to reconstruct the paleo-extent of ancient dammed lakes. As shown in Figure 1C and Table 1, section #1 and section #2 have the highest elevations of 3,187 m a.s.l. among the

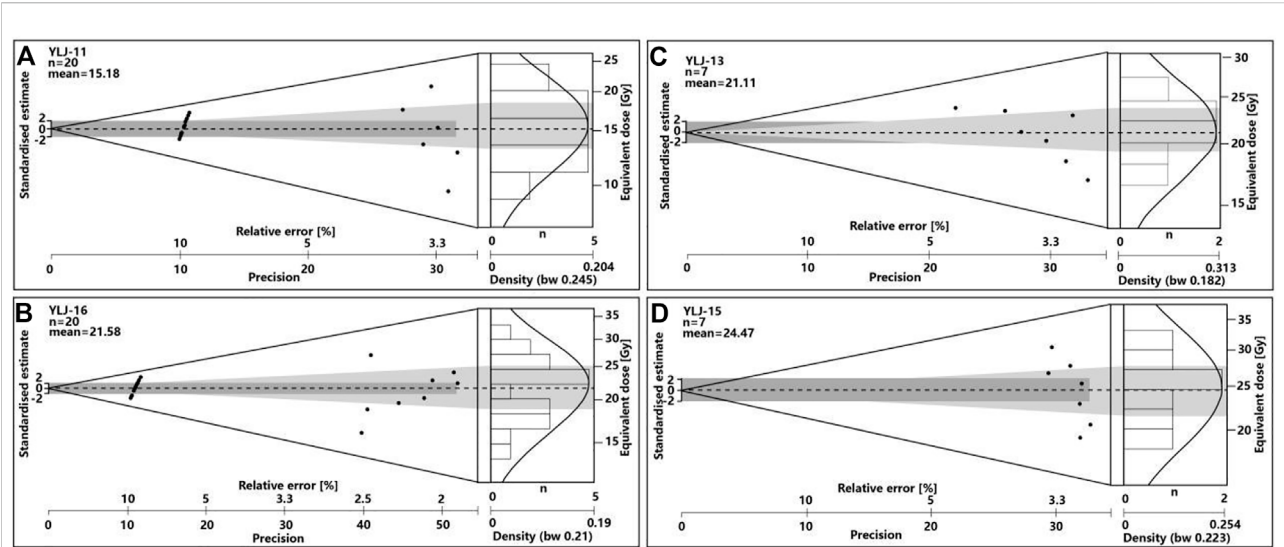


FIGURE 8

Equivalent dose distribution of samples in the Abanico plot (Dietze et al., 2016), which is a combination of radial, histogram, and probability density plots. (A–D) represent the Abanico plot of YLJ-11, YLJ-13, YLJ-16 and YLJ-15.

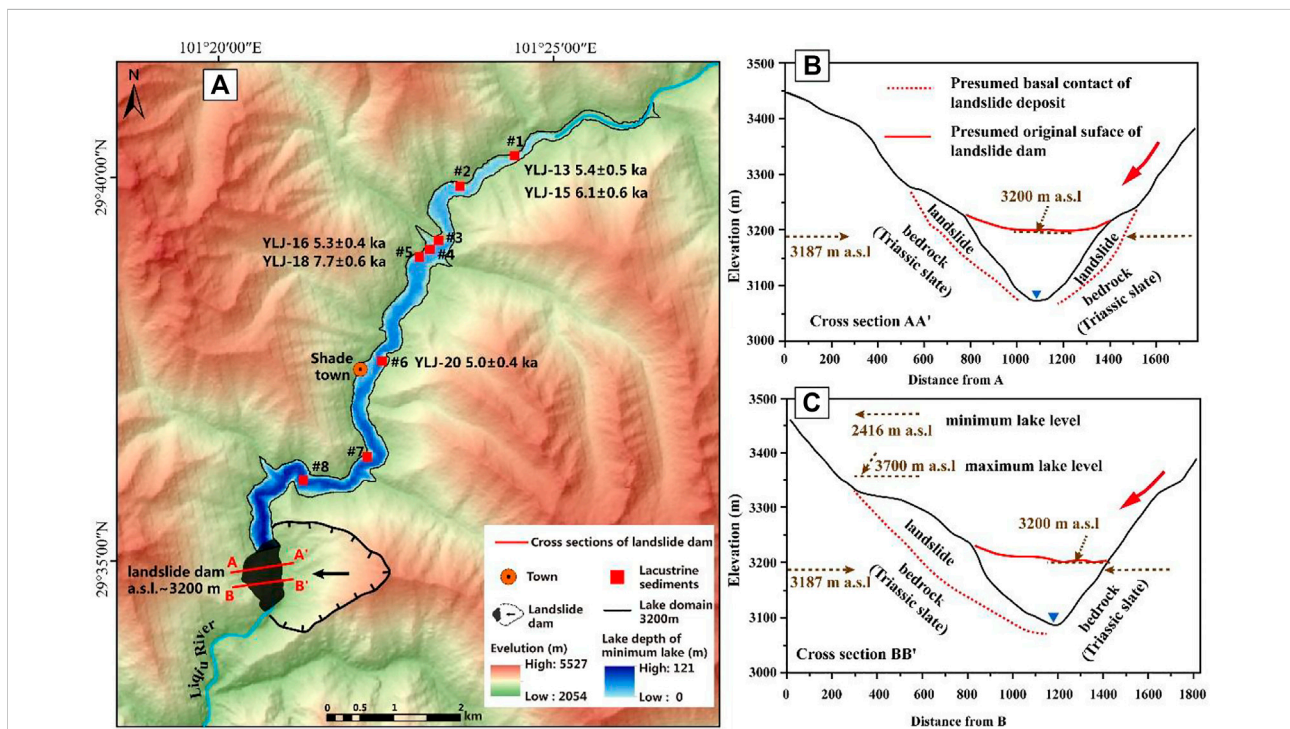


FIGURE 9

Paleo-extent and dam morphology of the Yuting landslide-dammed lake. (A) Paleo-extent of the minimum and maximum lake levels. The blue ramp shows the lake depth at a minimum lake level of 3,187 m a.s.l. The black line is the lake domain at the maximum lake derived at 3,200 m a.s.l. (B) and (C) Line graphs of cross-section AA' and cross-section BB'. The orientation of the cross-sections is marked in (A). They display the morphology of the lake outlet (relict dam), which illustrates the presumed original landslide surface and the dam height.

12 exposures in the reservoir area of the Yuting landslide-dammed lake. The upper climbing ripples overlying lacustrine clay varves in section #1[#] is indicative of the shallow water depth at this site or its adjacency to upstream inflow from the inundated river. Thus, the top elevation of section #1 (3,187 m a.s.l.) can represent the minimal lake level of the Yuting landslide-dammed lake, corresponding to a lake volume of $2.4 \times 10^8 \text{ m}^3$ and a lake area of 5.3 km². The maximum depth near the dam at a lake level of 3,187 m is approximately 115 m. Generally, the water depth at sites of other exposures, except section #2, increases in the downstream direction, ranging from 10 m to 65 m. This trend results from the travelling capacity of suspended silt or clay in the lake reservoir area.

On the other hand, the above analysis neglects that there may be an apparent water column present above the lake-bottom sediment as the lake ends. The elevations of lake-bottom sediments may underestimate lake levels (Johnsen and Brennand, 2004). Furthermore, it was proposed that 85% of landslide dams failed within 1 year (Costa and Schuster, 1988). It is possible that the lacustrine sediment in sections #1–#2 was deposited by relict lakes that had outburst earlier. We deduced the original or maximum lake level from the morphology of the remnant dam (Figures 9B,C). Cross-sections AA' and BB' display slightly rugged or undulating morphology on the left bank, which represents the landslide body. We extend the left-bank slope laterally toward the right to reconstruct the original elevation of the landslide dam, which is approximately 3,200 m a.s.l., giving a dam height of approximately 127 m. In other words, the Yuting landslide completely initially blocked the Liqiu River at 3,200 m a.s.l. The water volume of this original lake is approximately $3.2 \times 10^8 \text{ m}^3$, with an area of 6.2 km², the maximum estimate of the lake's extent.

The continuous deposition of clay varves suggests that the lake maintained relative stability over a long period from 7.7 ka BP to 3.9 ka BP. Considering the breaching behavior of the landslide-dammed lake proposed by Costa and Schuster (1988), we propose that the lake level of the Yuting landslide dam started to decrease due to incision as the lake water overtopped the dam, and then maintained stable as the water level lowered to 3,187 m a.s.l. The relict lake persisted for a sufficiently long period that the deposition rate at the upstream end surpassed that of the central lake. The aggradation in the location of section #1 contributed to a shallow marginal environment that facilitated the formation of climbing ripple deposition during 4.1–3.9 ka BP. At this time, the infill capacity was not reached at other locations of the Yuting landslide-dammed lake. However, nearly all of the OSL dates from clay varves, except for YLJ-10–YLJ-11 from climbing ripples, are concentrated in the period before 5.0 ka BP. As long as the infill capacity was not reached, it is impossible that the deposition at the location of sections #3–8 completely stopped between 5.0–3.9 ka BP. We

inferred that post-event erosion due to lateral migration of the river have erased the deposition in the upper parts of sections #3–8 during this period of time.

Furthermore, Ojala et al. (2012) constructed a varve database to study the fidelity of their varve chronologies. Among the 108 sites included in the varve database, varved records are typically 200–500 cm thick and cover a period of 1,000–2000 years. The thicknesses of annual varve may range from 0.07 to 27.3 mm/a, with a mean of 1.84 mm/a (Ojala et al., 2012). Assuming that the annual deposition rates of lacustrine sediments in the Yuting landslide-dammed lake are approximately 1.84 mm/y, the lacustrine thickness reaches 65 m, which is lower than the minimal estimation of maximal depth behind the landslide dam. This result indirectly confirms the reliability of the reconstructed paleo-extent.

5.2 Cause and trigger of the Yuting landslide-dammed lake

The stability of a bedrock slope can be affected by preparatory and triggering factors (Glade and Crozier, 2005). Preparatory factors, such as natural slopes oversteepening by river incision and glacier debuttressing, mainly reduce the stability over time but do not cause failure or movement (McCull, 2012). Triggering factors are those that initiate failure or movement, including rainfall, earthquakes, and sharp increases in porewater pressures (Cruden and Varnes, 1996; Jones et al., 2021). The Yuting landslide is located at a transitional position from a low-relief landscape perched ~2–2.5 km above the local base level into a rapidly incising, dissected landscape in its lower reaches [Figure 6 in Ouimet et al. (2007)]. The short-term (10^2 – 10^5 years) erosion rates in the upper reach of the Liqiu River range between 0.02 and 0.06 mm/a. However, the erosion rate increases to 0.40 mm/a downstream from the Yuting landslide (Ouimet et al., 2009). The rapid undercutting of hillslopes and mean local relief (up to 2 km) are high enough to focus topography-induced stresses that facilitate the occurrence of the Yuting landslide.

The watercourse of the Liqiu River develops along the Shade fault, which passes through the source area of the Yuting landslide. The slip rate and paleo-seismic activity of the Shade faults remain unknown. However, it is adjacent to the Xianshuihe fault system, which has given rise to 59 $M_s \geq 5.0$ earthquakes since 1725, including 18 $M_s \geq 6.0$ –6.9 and eight ≥ 7.0 earthquakes (Zhang et al., 2016). Ma et al. (2022) revealed six Holocene paleoearthquake events that occurred from approximately 7,168–6,269 and 3,465–2,490 years BP near Kangding, which is outside the range of the initiating and ending times of the Yuting landslide-dammed lake. This temporal inconsistency may imply that the reconstructed damming event was not

triggered by earthquakes. As with the similar cases of Tanggudong landslide and Baige landslide, the intensive crustal uplift and the rapid river erosion have markedly altered the free face of the damaged rock mass, thereby increasing the gravitational potential energy of the rock mass (Yi et al., 2022). The long-term cumulative coupled effect of tectonic movement and surface denudation represents the fundamental mechanism of the Yuting landslides.

6 Conclusion

We revealed 12 exposures associated with an ancient lake formed by the Yuting landslide blocking the Liqiu River in the middle reach of the Yalong River. The sedimentary evidence mainly consists of typical clay or silt varves deposited in deep water. Locally, the Bouma sequence develops due to subaqueous turbidity flows and climbing ripples. The elevation distributions of 12 exposures and sedimentary analysis determine the minimal estimate of the paleo-extent of this ancient lake, which is at 3,187 m a.s.l., giving a volume of $2.4 \times 10^8 \text{ m}^3$. The dam morphology further provides the maximum estimate of the lake extent at 3,200 m a.s.l., with a lake volume of $3.2 \times 10^8 \text{ m}^3$. In total, we obtained 12 OSL ages collected from three sections. An Abanico plot was used to test the error introduced by partial bleaching of the OSL signal. Except for three OSL ages, the OSL signals of the others are adequately zeroed. The results illustrate that the Yuting landslide-dammed lake initiated before 7.9 ka BP and persisted until at least 3.9 ka BP. This chronological limit should be considered the minimum lifespan of the Yuting landslide-dammed lake, which may have formed earlier and persisted longer. A small discrepancy exists between the original dam height recovered from the morphology of the landslide body and the water depth represented by the highest lacustrine sediment. We suggest that an initial drainage occurred as the lake water overtopped the landslide dam, which lowered the highstand lake surface at 3,200 m a.s.l. to a long-lasting water level at 3,187 m a.s.l. The long-term cumulative coupled effect of tectonic movement and the rapid river incision rate provided favorable conditions for the failure of the Yuting landslide.

References

- Baker, V. R. (2020). "Global megaflood paleohydrology," in *Palaeohydrology: Traces, tracks and trails of extreme events*. Editors J. Herget and A. Fontana (Cham: Springer International Publishing), 3–28.
- Baker, V. R. (2009). The channeled scabland: A retrospective. *Annu. Rev. Earth Planet. Sci.* 37, 393–411. doi:10.1146/annurev.earth.061008.134726
- Bao, Y., Zhai, S., Chen, J., Xu, P., Sun, X., Zhan, J., et al. (2020). The evolution of the Samaoding paleolandslide river blocking event at the upstream reaches of the Jinsha River, Tibetan Plateau. *Geomorphology* 351, 106970. doi:10.1016/j.geomorph.2019.106970
- Baynes, E. R., Attal, M., Niedermann, S., Kirstein, L. A., Dugmore, A. J., and Naylor, M. (2015). Erosion during extreme flood events dominates Holocene

Data availability statement

The original contributions presented in the study are included in the article/Supplementary Material; further inquiries can be directed to the corresponding author.

Author contributions

HW: conceptualization, investigation, writing—original draft, funding acquisition; AY: methodology, software, formal analysis, investigation, writing—original draft; SJ: methodology, software, data curation; NL: software, formal analysis, data curation.

Funding

This research was supported by the Second Tibetan Plateau Scientific Expedition and Research Program (STEP) (Grant No. 2019QZKK0906), the Sichuan Province Science and Technology Support Program (Grant No. 2021YFH0009), and the National Natural Science Foundation of China (Grant Nos 41941017 and 42101083).

Conflict of interest

The authors declare that the research was conducted in the absence of any commercial or financial relationships that could be construed as a potential conflict of interest.

Publisher's note

All claims expressed in this article are solely those of the authors and do not necessarily represent those of their affiliated organizations or those of the publisher, the editors, and the reviewers. Any product that may be evaluated in this article, or claim that may be made by its manufacturer, is not guaranteed or endorsed by the publisher.

canyon evolution in northeast Iceland. *Proc. Natl. Acad. Sci. U. S. A.* 112 (8), 2355–2360. doi:10.1073/pnas.1415443112

Bazai, N. A., Cui, P., Carling, P. A., Wang, H., Hassan, J., Liu, D., et al. (2021). Increasing glacial lake outburst flood hazard in response to surge glaciers in the Karakoram. *Earth-Science Rev.* 212, 103432–103521. doi:10.1016/j.earscirev.2020.103432

Cantero, M. I., Cantelli, A., Pirmez, C., Balachandar, S., Mohrig, D., Hickson, T. A., et al. (2012). Emplacement of massive turbidites linked to extinction of turbulence in turbidity currents. *Nat. Geosci.* 5 (1), 42–45. doi:10.1038/ngeo1320

Carling, P. A. (2013). Freshwater megaflood sedimentation: What can we learn about generic processes? *Earth-Science Rev.* 125, 87–113. doi:10.1016/j.earscirev.2013.06.002

- Chen, J., Dai, F., Lv, T., and Cui, Z. (2013). Holocene landslide-dammed lake deposits in the Upper Jinsha River, SE Tibetan Plateau and their ages. *Quat. Int.* 298, 107–113. doi:10.1016/j.quaint.2012.09.018
- Chen, J., Dai, F., and Yao, X. (2008). Holocene debris-flow deposits and their implications on the climate in the upper Jinsha River valley, China. *Geomorphology* 93 (3–4), 493–500. doi:10.1016/j.geomorph.2007.03.011
- Chen, Y. J., Zhou, F., Feng, Y., and Xia, Y. C. (1992). Breach of a naturally embanked dam on Yalong River. *Can. J. Civ. Eng.* 19 (5), 811–818. doi:10.1139/l92-092
- Costa, J. E., and Schuster, R. L. (1988). The formation and failure of natural dams. *Geol. Soc. Am. Bull.* 100 (7), 1054–1068. doi:10.1130/0016-7606(1988)100<1054:tfafon>2.3.co;2
- Cruden, D., and Varnes, D. J. (1996). “Landslide types and processes,” in *Landslides: Investigation and mitigation*. Editors A. K. Turner and R. L. Schuster (Washington, DC: National Academy Press), 36–75.
- Delaney, K. B., and Evans, S. G. (2015). The 2000 Yigong landslide (Tibetan Plateau), rockslide-dammed lake and outburst flood: Review, remote sensing analysis, and process modelling. *Geomorphology* 246, 377–393. doi:10.1016/j.geomorph.2015.06.020
- Dietze, M., Kreutzer, S., Burow, C., Fuchs, M. C., Fischer, M., and Schmidt, C. (2016). The abanico plot: Visualising chronometric data with individual standard errors. *Quat. Geochronol.* 31, 12–18. doi:10.1016/j.quageo.2015.09.003
- Ding, Y., Zhang, X., He, Z., Lu, C., and Bao, S. (2021). Sedimentary environment of a dammed lake buried in the modern riverbed of the Yalong River during the Last Glacial Maximum and its implication for fluvial geomorphic evolution. *Geomorphology* 378, 107588. doi:10.1016/j.geomorph.2020.107588
- Fan, A., Li, S. H., and Li, B. (2011). Observation of unstable fast component in OSL of quartz. *Radiat. Meas.* 46 (1), 21–28. doi:10.1016/j.radmeas.2010.10.001
- Feng, X. F., Yang, Q. Y., Zhang, O. Y., and Wang, X. K. (2008). Sediment trap of eretan reservoir and its effect on sediment budget of Jinsha River. *J. Sichuan Univ. Eng. Sci. Ed.* 40, 37–42.
- Glade, T., and Crozier, M. J. (2005). “The nature of landslide hazard impact” in *Landslide Hazard and Risk*, Editors T. Glade, M. Anderson, and M. J. Crozier (Chichester: Wiley), 41–74.
- Hayles, S., Al, T., Cornett, J., Harrison, A., and Zhao, J. (2021). Growth rates for freshwater ferromanganese concretions indicate regional climate change in eastern Canada at the Northgrippian-Meghalayan boundary. *Holocene* 31 (8), 1250–1263. doi:10.1177/09596836211011652
- Hu, K., Wei, L., Yang, A., Wu, C., Zhang, Q., Liu, S., et al. (2022). Broad valleys and barrier dams in upstream Brahmaputra efficiently retain Tibetan-sourced sediments: Evidence from palaeoflood records. *Quat. Sci. Rev.* 285, 107538. doi:10.1016/j.quascirev.2022.107538
- Johnsen, T. F., and Brennand, T. A. (2004). Late-glacial lakes in the thompson basin, British Columbia: Paleogeography and evolution. *Can. J. Earth Sci.* 41 (11), 1367–1383. doi:10.1139/e04-074
- Jones, J. N., Boulton, S. J., Bennett, G. L., Stokes, M., and Whitworth, M. R. Z. (2021). Temporal variations in landslide distributions following extreme events: Implications for landslide susceptibility modeling. *J. Geophys. Res. Earth Surf.* 126 (7). doi:10.1029/2021j006067
- Korup, O., Densmore, A. L., and Schlunegger, F. (2010). The role of landslides in mountain range evolution. *Geomorphology* 120 (1–2), 77–90. doi:10.1016/j.geomorph.2009.09.017
- Korup, O., and Montgomery, D. R. (2008). Tibetan plateau river incision inhibited by glacial stabilization of the Tsangpo gorge. *Nature* 455 (7214), 786–789. doi:10.1038/nature07322
- Lai, Z., and Brückner, H. (2008). Effects of feldspar contamination on equivalent dose and the shape of growth curve for OSL of silt-sized quartz extracted from Chinese loess. *Geochronometria.* 30, 49–53. doi:10.2478/v10003-008-0010-0
- Lai, Z., Kaiser, K., and Brückner, H. (2009). Luminescence-dated aeolian deposits of late Quaternary age in the southern Tibetan Plateau and their implications for landscape history. *Quaternary Research* 72 (3), 421–430.
- Lai, Z., Mischke, S., and Madsen, D. (2014). Paleoenvironmental implications of new OSL dates on the formation of the “shell bar” in the qaidam basin, northeastern qinghai-Tibetan plateau. *J. Paleolimnol.* 51 (2), 197–210. doi:10.1007/s10933-013-9710-1
- Lai, Z., and Ou, X. (2013). Basic procedures of optically stimulated luminescence (OSL) dating. *Prog. Geogr.* 32, 683–693.
- Lai, Z. (2006). Testing the use of an OSL standardised growth curve (SGC) for determination on quartz from the Chinese Loess Plateau. *Radiat. Meas.* 41 (1), 9–16. doi:10.1016/j.radmeas.2005.06.031
- Lang, J., Brandes, C., and Winsemann, J. (2017). Erosion and deposition by supercritical density flows during channel avulsion and backfilling: Field examples from coarse-grained deepwater channel-levée complexes (Sandino Forearc Basin, southern Central America). *Sediment. Geol.* 349, 79–102. doi:10.1016/j.sedgeo.2017.01.002
- Lang, J., and Winsemann, J. (2013). Lateral and vertical facies relationships of bedforms deposited by aggrading supercritical flows: From cyclic steps to humpback dunes. *Sediment. Geol.* 296 (14), 36–54. doi:10.1016/j.sedgeo.2013.08.005
- Lapointe, F., Francus, P., Stoner, J. S., Abbott, M. B., Balascio, N. L., Cook, T. L., et al. (2019). Chronology and sedimentology of a new 2.9 ka annually laminated record from south sawtooth lake, ellesmere island in this NOAA depository: <https://www.ncdc.noaa.gov/paleo/study/33214>. *Quat. Sci. Rev.* 222, 105875. doi:10.1016/j.quascirev.2019.105875
- Larsen, I. J., and Lamb, M. P. (2016). Progressive incision of the Channeled Scablands by outburst floods. *Nature* 538 (7624), 229–232. doi:10.1038/nature19817
- Larsen, I. J., Montgomery, D. R., and Korup, O. (2010). Landslide erosion controlled by hillslope material. *Nat. Geosci.* 3 (4), 247–251. doi:10.1038/ngeo776
- Letéron, A., Hamon, Y., Fournier, F., Séranne, M., Pellenard, P., and Joseph, P. (2018). Reconstruction of a saline, lacustrine carbonate system (Priabonian, St-Chaptes Basin, SE France): Depositional models, paleogeographic and paleoclimatic implications. *Sediment. Geol.* 367, 20–47. doi:10.1016/j.sedgeo.2017.12.023
- Li, S.-L., Chetelat, B., Yue, F., Zhao, Z., and Liu, C.-Q. (2014). Chemical weathering processes in the Yalong River draining the eastern Tibetan Plateau, China. *J. Asian Earth Sci.* 88, 74–84. doi:10.1016/j.jseas.2014.03.011
- Li, Y., Chen, J., Zhou, F., Song, S., Zhang, Y., Gu, F., et al. (2020). Identification of ancient river-blocking events and analysis of the mechanisms for the formation of landslide dams in the Suwalong section of the upper Jinsha River, SE Tibetan Plateau. *Geomorphology* 368, 107351. doi:10.1016/j.geomorph.2020.107351
- Liu, D., Cui, Y., Wang, H., Jin, W., Wu, C., Bazai, N. A., et al. (2021). Assessment of local outburst flood risk from successive landslides: Case study of Baige landslide-dammed lake, upper Jinsha river, eastern Tibet. *J. Hydrology* 599, 126294. doi:10.1016/j.jhydrol.2021.126294
- Liu, W., Carling, P. A., Hu, K., Wang, H., Zhou, Z., Zhou, L., et al. (2019). Outburst floods in China: A review. *Earth-Science Rev.* 197, 102895. doi:10.1016/j.earscirev.2019.102895
- Liu, W., Hu, K., Carling, P. A., Lai, Z., Cheng, T., and Xu, Y. (2018). The establishment and influence of Baimakou paleo-dam in an upstream reach of the Yangtze River, southeastern margin of the Tibetan Plateau. *Geomorphology* 321, 167–173. doi:10.1016/j.geomorph.2018.08.028
- Liu, W., Lai, Z., Hu, K., Ge, Y., Cui, P., Zhang, X., et al. (2015). Age and extent of a giant glacial-dammed lake at Yarlung Tsangpo gorge in the Tibetan Plateau. *Geomorphology* 246, 370–376. doi:10.1016/j.geomorph.2015.06.034
- Liu, X., Lai, Z., Yu, L., Sun, Y., and Madsen, D. (2012). Luminescence chronology of aeolian deposits from the Qinghai Lake area in the Northeastern Qinghai-Tibetan Plateau and its palaeoenvironmental implications. *Quaternary Geochronology* 10, 37–43.
- Ma, J., Wang, M., Ha, G., Lei, J., and Zhou, B. (2022). Latest quaternary active faulting and paleoearthquakes on the yalaha fault of the Xianshuihe fault zone, eastern Tibetan plateau. *Tectonophysics* 837, 229448. doi:10.1016/j.tecto.2022.229448
- Mangerud, J., Astakhov, V. I., Murray, A., and Svendsen, J. I. (2001). The chronology of a large ice-dammed lake and the Barents-Kara Ice Sheet advances, Northern Russia. *Glob. Planet. Change* 31 (1), 321–336. doi:10.1016/s0921-8181(01)00127-8
- McColl, S. T. (2012). Paraglacial rock-slope stability. *Geomorphology* 153–154, 1–16. doi:10.1016/j.geomorph.2012.02.015
- Murray, A. S., Olley, J. M., and Caitcheon, G. G. (1995). Measurement of equivalent doses in quartz from contemporary water-lain sediments using optically stimulated luminescence. *Quat. Sci. Rev.* 14 (4), 365–371. doi:10.1016/0277-3791(95)00030-5
- Murray, A. S., and Wintle, A. G. (2000). Luminescence dating of quartz using an improved single-aliquot regenerative-dose protocol. *Radiat. Meas.* 32 (1), 57–73. doi:10.1016/s1350-4487(99)00253-x
- Ojala, A. E. K., Francus, P., Zolitschka, B., Besonen, M., and Lamoureux, S. F. (2012). Characteristics of sedimentary varve chronologies – a review. *Quat. Sci. Rev.* 43, 45–60. doi:10.1016/j.quascirev.2012.04.006
- Olley, J., Caitcheon, G. G., and Roberts, R. (1999). The origin of dose distributions in fluvial sediments, and the prospect of dating single grains from fluvial deposits using optically stimulated luminescence. *Radiat. Meas.* 30 (2), 207–217. doi:10.1016/s1350-4487(99)00040-2

- Olley, J., Caitcheon, G., and Murray, A. (1998). The distribution of apparent dose as determined by Optically Stimulated Luminescence in small aliquots of fluvial quartz: Implications for dating young sediments. *Quat. Sci. Rev.* 17 (11), 1033–1040. doi:10.1016/s0277-3791(97)00090-5
- Ouimet, W. B., Whipple, K. X., and Granger, D. E. (2009). Beyond threshold hillslopes: Channel adjustment to base-level fall in tectonically active mountain ranges. *Geology* 37 (7), 579–582. doi:10.1130/g30013a.1
- Ouimet, W. B., Whipple, K. X., Royden, L. H., Sun, Z., and Chen, Z. (2007). The influence of large landslides on river incision in a transient landscape: Eastern margin of the Tibetan Plateau (Sichuan, China). *Geol. Soc. Am. Bull.* 119 (11–12), 1462–1476. doi:10.1130/b26136.1
- Pietsch, T. J., Olley, J. M., and Nanson, G. C. (2008). Fluvial transport as a natural luminescence sensitizer of quartz. *Quat. Geochronol.* 3 (4), 365–376. doi:10.1016/j.quageo.2007.12.005
- Prescott, J. R., and Hutton, J. T. (1994). Cosmic ray contributions to dose rates for luminescence and ESR dating: Large depths and long-term time variations. *Radiat. Meas.* 23 (2), 497–500. doi:10.1016/1350-4487(94)90086-8
- Preusser, F., Andersen, B. G., Denton, G. H., and Schlüchter, C. (2005). Luminescence chronology of late pleistocene glacial deposits in north westland, New Zealand. *Quat. Sci. Rev.* 24 (20–21), 2207–2227. doi:10.1016/j.quascirev.2004.12.005
- Preusser, F., Chithambo, M. L., Götte, T., Martini, M., Ramseyer, K., Sendezera, E. J., et al. (2009). Quartz as a natural luminescence dosimeter. *Earth-Science Rev.* 97 (1–4), 184–214. doi:10.1016/j.earscirev.2009.09.006
- Preusser, F., Ramseyer, K., and Schlüchter, C. (2006). Characterisation of low OSL intensity quartz from the New Zealand Alps. *Radiat. Meas.* 41 (7–8), 871–877. doi:10.1016/j.radmeas.2006.04.019
- Roberts, H. M., and Duller, G. A. T. (2004). Standardised growth curves for optical dating of sediment using multiple-grain aliquots. *Radiat. Meas.* 38 (2), 241–252. doi:10.1016/j.radmeas.2003.10.001
- Russell, H. A. J., and Arnott, R. W. C. (2003). Hydraulic-jump and hyperconcentrated-flow deposits of a glacial subaqueous fan: Oak ridges moraine, southern ontario, Canada. *J. Sediment. Res.* 73 (6), 887–905. doi:10.1306/041103730887
- Simonett, D. S. (1967). *Landslide distribution and earthquakes in the bavani and torricelli mountains*. New Guinea: Landform studies from Australia and New Guinea, 64–84.
- Steffen, D., Preusser, F., and Schlunegger, F. (2009). OSL quartz age underestimation due to unstable signal components. *Quat. Geochronol.* 4 (5), 353–362. doi:10.1016/j.quageo.2009.05.015
- Wallinga, J. (2002). Optically stimulated luminescence dating of fluvial deposits: A review. *Boreas* 31 (4), 303–322. doi:10.1080/030094802320942536
- Wang, H., Cui, P., Liu, D., Liu, W., Bazai, N. A., Wang, J., et al. (2019). Evolution of a landslide-dammed lake on the southeastern Tibetan Plateau and its influence on river longitudinal profiles. *Geomorphology* 343, 15–32. doi:10.1016/j.geomorph.2019.06.023
- Wang, H., Cui, P., Zhou, L., Liu, W., Yang, A., Yao, S., et al. (2022). Spatial and temporal distribution of landslide-dammed lakes in Purlung Tsangpo. *Eng. Geol.* 308, 106802. doi:10.1016/j.enggeo.2022.106802
- Wang, P., Chen, J., Dai, F., Long, W., Xu, C., Sun, J., et al. (2014). Chronology of relict lake deposits around the Suwalong paleolandslide in the upper Jinsha River, SE Tibetan Plateau: Implications to Holocene tectonic perturbations. *Geomorphology* 217, 193–203. doi:10.1016/j.geomorph.2014.04.027
- Wang, Y., Lei, X., Wen, X., Fang, G., Tan, Q., Tian, Y., et al. (2019). Effects of damming and climatic change on the eco-hydrological system: A case study in the Yalong River, southwest China. *Ecol. Indic.* 105, 663–674. doi:10.1016/j.ecolind.2018.07.039
- Winsemann, J., Lang, J., Polom, U., Loewer, M., Igel, J., Pollok, L., et al. (2018). Ice-marginal forced regressive deltas in glacial lake basins: Geomorphology, facies variability and large-scale depositional architecture. *Boreas* 47, 973–1002. doi:10.1111/bor.12317
- Yang, A., Wang, H., Liu, W., Hu, K., Liu, D., Wu, C., et al. (2022). Two megafloods in the middle reach of Yarlung Tsangpo River since Last-glacial period: Evidence from giant bars. *Glob. Planet. Change* 208, 103726. doi:10.1016/j.gloplacha.2021.103726
- Yi, S., Wu, C., Cui, P., Li, Y., and Lei, M. (2022). Cause of the Baige landslides: Long-term cumulative coupled effect of tectonic action and surface erosion. *Lithosphere* 2021. (Special 7). doi:10.2113/2022/7784535
- Zhang, Y., Yao, X., Yu, K., Du, G., and Guo, C. (2016). Late-Quaternary slip rate and seismic activity of the Xianshuihe fault zone in southwest China. *Acta Geol. Sin. - Engl. Ed.* 90 (2), 525–536. doi:10.1111/1755-6724.12688
- Zhang, Y., Zhao, X., Lan, H., and Xiong, T. (2011). A pleistocene landslide-dammed lake, Jinsha River, yunnan, China. *Quat. Int.* 233 (1), 72–80. doi:10.1016/j.quaint.2010.10.020
- Zolitschka, B., Francus, P., Ojala, A. E. K., and Schimmelmann, A. (2015). Varves in lake sediments – A review. *Quat. Sci. Rev.* 117, 1–41. doi:10.1016/j.quascirev.2015.03.019